Journal of Marine Science and Technology

Volume 27 | Issue 3 Article 1

NUMERICAL AND EXPERIMENTAL PREDICTION OF HYDRODYNAMIC INTERACTION EFFECTS ACTING ON TUGS DURING SHIP MANOEUVRES

Nirman Jayarathne
Australian Maritime College, Specialist Institute of the Universityof Tasmania,Australia. General Sir John Kotelawala Defence University, Ratmalana, Sri Lanka.

Dev Ranmuthugala
Australian Maritime College, Specialist Institute of the Universityof Tasmania, Australia.

Zhi Leong
Australian Maritime College, Specialist Institute of the Universityof Tasmania, Australia.

Jiangang Fei
Australian Maritime College, Specialist Institute of the Universityof Tasmania, Australia

Shuhong Chai
Australian Maritime College, Specialist Institute of the Universityof Tasmania, Australia

NUMERICAL AND EXPERIMENTAL PREDICTION OF HYDRODYNAMIC INTERACTION EFFECTS ACTING ON TUGS DURING SHIP MANOEUVRES

Acknowledgements

Authors would like to thank AMC model test basin staff for their valuable support during the experiments.

Journal of Marine Science and Technology, Vol. 27, No. 3, pp. 185-201 (2019)
DOI: 10.6119/JMST.201906_27(3).0001

NUMERICAL AND EXPERIMENTAL PREDICTION OF HYDRODYNAMIC INTERACTION EFFECTS ACTING ON TUGS DURING SHIP MANOEUVRES

Nirman Jayarathne[1, 2], Dev Ranmuthugala[1],
Zhi Leong[1], Jiangang Fei[1], and Shuhong Chai[1]

Key words: CFD and EFD, ship interaction, turbulence model, near wall mesh.

ABSTRACT

The role of tug boats is significant when assisting ships with limited manoeuvring capabilities. Hence, knowledge of the hydrodynamic interaction effects that act on a tug under these operations is of great practical value for the tug master in order to avoid damage, collision, or capsizing. Computational Fluid Dynamic (CFD) simulations are increasingly being adopted as a tool of analysis for determining the interaction effects in such vessel manoeuvres. However, one of the major challenges faced in CFD, is that the results can vary greatly depending on the numerical model settings. This paper investigates modelling techniques and the accuracy of CFD generated interaction forces and moments acting on a tug hull operating at different drift angles, and at lateral and longitudinal locations along a tanker hull against Experimental Fluid Dynamics (EFD) data.

I. INTRODUCTION

The role of tug boats is significant when assisting ships with limited manoeuvring capabilities at slow speeds in restricted waters. However, the hydrodynamic interaction between these vessels can adversely affect the handling and safety of the much smaller tugs, which in extreme cases can lead to the latter capsizing or colliding. "Dangers of interaction" (MCA, 2001) is a guidance note prepared by the Maritime Coastguard Agency in the United Kingdom to draw the attention of ship owners, pilots, and ship and tug masters to the effects of hydrodynamic interaction on vessel manoeuvrability. It states that when vessels are being manoeuvred at close quarters for operational reasons, the greatest potential danger exists when there is a large difference in size between the two vessels and it is most commonly experienced when a ship is being attended by a tug (MCA, 2001).

The Marine Accident Investigation Branch (MAIB, 2011) report strongly suggests mariners to familiarise themselves with the 'Dangers of interaction' guideline in order to be alert to dangerous situations caused by hydrodynamic interaction effects during these operations. One aspect of the training to meet these requirements is the use of appropriate simulators for those who operate ships and tugs, to familiarize themselves with interaction effects during critical manoeuvres. For these simulators to replicate actual behaviour, it is essential that the interaction effects are accurately determined by mathematical models to provide seafarers with realistic experiences. However, the pursuit of accuracy should not affect the ability to provide real-time responses within simulators. Thus, many studies such as: Vantorre et al. (2002), Sorensen et al. (2009), Falter (2010), Geerts et al. (2011), Lindberg et al. (2012), Sutulo et al. (2012), Pinkster and Bhawsinka (2013) have been carried out to improve predictions of the interaction effects in simulators, without adversely affecting their accuracy and real-time responses.

Sutulo et al. (2012) identified potential flow theory as one of the best methods for the prediction of real time interaction effects within simulators. They conducted model scale experiments to measure the interaction effects acting on an azimuth stern drive tug operating in close proximity to a conventional tanker. These tests were conducted in both shallow and deep water using a tug model placed in various heading angles and positions around the tanker model. However, only those where the vessels were parallel to each other (referred to as parallel operations) were compared and discussed against the potential flow code results in their study. The results illustrated the capability of the potential flow method to predict interaction effects, while highlighting a lack of accuracy in predicting the sway force and yaw moment at small horizontal clearances, which was expected to be more pronounced in non-parallel operations, i.e., vessels with different drift angles. These findings were supported by work carried out by the authors through comparative numerical and experimental investigations that identified inaccuracies of the

Paper submitted 16/11/16; revised 14/02/17; accepted 10/04/17. Author for correspondence: Hong-Ming Chen (e-mail: hmchen@mail.ntou.edu.tw).
[1] *Australian Maritime College, Specialist Institute of the Universityof Tasmania, Australia.*
[2] *General Sir John Kotelawala Defence University, Ratmalana, Sri Lanka.*

forces along the hull calculated by potential flow methods for a tug boat with a transom stern hull (Jayarathne et al., 2014). The study also showed that the results obtained through Reynolds Averaged Navier-Stokes (RANS) based Computational Fluid Dynamics (CFD) simulations were in good agreement with the experimental measurement.

A CFD based study of the interaction between a tug and a large tanker sailing in parallel was undertaken by Fonfach et al. (2011). They used inviscid flow, turbulent viscous flow, inviscid free surface flow, and viscous free surface flow theories with Standard Spalart-Allmaras (SA) and Shear Stress Transport (SST) turbulence models in their study. The target cell size near the tug was maintained as 0.0025 times the tug length. They observed large discrepancies in the results predicted by all flow models at small lateral clearances, especially for the sway force. Due to time constraints, the authors did not conduct a mesh convergence study in their investigation, thus the accuracy of the selected turbulence model and the near wall cell size cannot be verified with the available data. Nevertheless, their results showed that the CFD model with both the viscous and free surface effects had better agreement with experimental data compared to the other flow theories utilized.

Simonsen et al. (2011) did a CFD based study on a subset of cases taken from model scale experiments studying quasi-steady ship-to-ship interaction effects. A tug was located at a number of longitudinal and transverse positions alongside a tanker for parallel operations. However, it was locked near the midship of the tanker for the drifted tug analysis, with the tug angle varying from 0 to 60 degrees. The authors had done a semi-systematic refinement for the initial CFD grid and checked the trend of the solution, with the non-dimensional wall distance of first inflation layer (y) on the no-slip surfaces for the simulations maintained between 1 and 30 with the SST turbulence model. Their CFD results showed poor agreement with the experimental data for the sway force acting on the tug at selected tug drift angles. The cause of the error was inconclusive as the study did not quantify the experimental or numerical uncertainties.

In this way, a number of researchers have used experimental and CFD methods to predict forces and moments acting on tugs during ship handling. However, their investigations have covered only limited operational scenarios including parallel operation and limited drift angles at fixed locations relative to the larger vessel. Furthermore, the numerical and experimental uncertainties were not clearly quantified when making comparisons against experimental work. Therefore, the causes of the discrepancies between CFD and the experimental data are hard to identify. This paper extends the above findings by investigating the capability of CFD to predict interaction effects acting on tugs during ship handling at parallel and drifted operations at different lateral and longitudinal locations along a tanker (i.e., the larger vessel). The CFD simulation results generated by Star-CCM+® for different tug-ship combinations were compared against captive model scale test results obtained via a series of experiments conducted in the model test basin at the Australian Maritime College (AMC). Finally, the paper explores the effect of the CFD modelling factors, such as the selection of turbulence model, application of y in the near-wall mesh, and the quality of the mesh model on force and moment predictions.

Table 1. Principal dimensions of the selected hull forms.

Main Particulars	Unit	Tanker		Tug	
		Full Scale	Model Scale	Full Scale	Model Scale
Length Overall	m	75.60	4.20	31.16	1.732
Length Waterline	m	72.00	4.00	28.46	1.581
Breadth	m	13.12	0.729	11.50	0.639
Draft	m	4.43	0.246	3.54	0.197
Scale	-	1	1/18	1	1/18

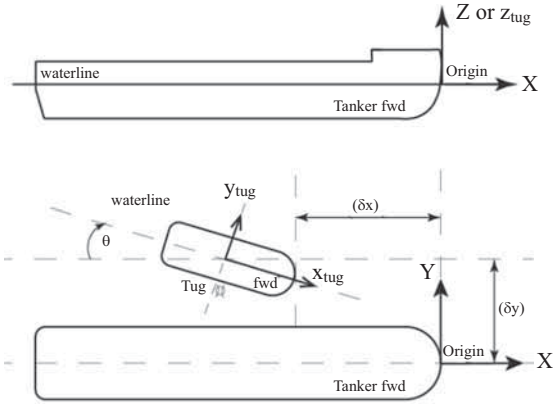

Fig. 1. Local (tug) and global coordinate systems and vessel locations.

II. NUMERICAL SIMULATIONS

1. Selection of Ship Models

For the study of tug-ship interaction, the CFD simulations consisted of generic model scale hulls of a stern drive tug and a MARAD-F series tanker with a length ratio of 1:2.4 between the two vessels. The vessel particulars are given in Table 1 and the coordinate system for the analysis is shown in Fig. 1.

Throughout the analysis the tug was located on the port side of the tanker, with a range of lateral distances (δ_y) and longitudinal locations (δ_x) as shown in Fig. 1.

The three-dimensional model scale hull form geometries were developed using the commercial software Rhinoceros® V5.0 as shown in Fig. 2 and imported into Star-CCM+®.

2. Non-Dimensionalisation of Results

The hydrodynamic surge force (X), sway force (Y), and yaw moment (N) acting on the tug were non-dimensionalised for CFD and EFD comparisons based on the volumetric displacements of hulls using Eqs. (1)-(3) as previously employed in similar studies (Sutulo and Soares, 2009; Fonfach et al., 2011; Simonsen et al., 2011).

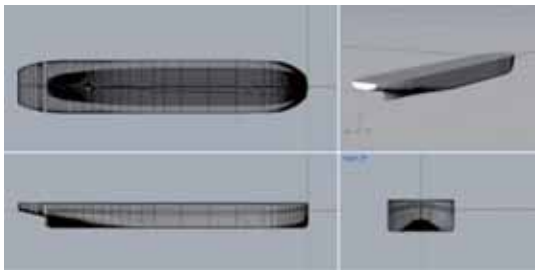

(a) MARAD-F series tanker

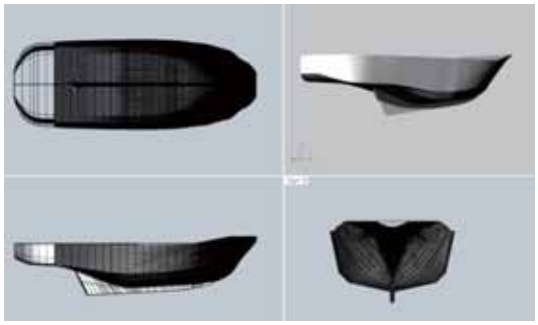

(b) stern drive tug

Fig. 2. 3D hull forms.

$$C_X = \frac{2X}{u^2 \nabla_t^{1/3} \nabla_s^{1/3} \rho} \tag{1}$$

$$C_Y = \frac{2Y}{u^2 \nabla_t^{1/3} \nabla_s^{1/3} \rho} \tag{2}$$

$$C_N = \frac{2N}{u^2 \nabla_t^{1/3} \nabla_s^{1/3} L_t \rho} \tag{3}$$

The lateral (ΔY) and longitudinal locations (ΔX) of the tug were also non-dimensionalised using tanker dimensions as defined in Eq. (4) and Eq. (5) respectively (Sutulo and Soares, 2009; Fonfach et al., 2011; Simonsen et al., 2011).

$$\Delta Y = \frac{\delta y}{B_s} \tag{4}$$

$$\Delta X = \frac{2\delta x}{L_s} \tag{5}$$

3. Numerical Setup

The finite volume based Star-CCM+® package was used to solve the RANS equations employing three different turbulence models, i.e., Realizable Two Layer k-ε (RKE), Shear Stress Transport (SST), and Spalart-Allmaras (SA) (CD-Adapco, 2015). However, for the mesh sensitivity study, only the SST

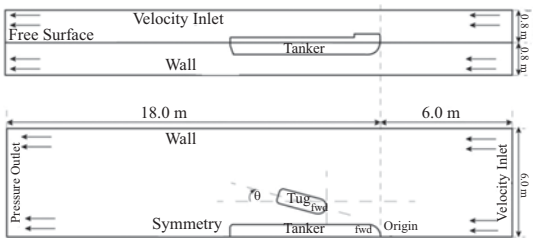

Fig. 3. Computational domain used in Star-CCM+® simulations.

turbulence model was utilized. The implicit unsteady simulations were carried out with the free surface modelled as an Euler Multiphase, using the Volume of Fluid technique (CD-Adapco, 2015). For the accuracy of results, it is important to establish a suitable grid after evaluating the effects of the total thickness of inflation layers around the tug boat and y of the first inflation layer. Leong et al. (2014) verified that the thickness of the inflation layers around a body should be at least 1.5 times of Prandtl's 1/7th power law ($1.5 \times 0.16 L_t / Re_{Lt}^{1/7}$) estimate of a turbulence boundary layer thickness over the surface length. Thus in this study, the total thickness of the boundary layer was maintained as 2.0 times Prandtl's 1/7th power law estimate, and inbuilt prism layer mesher (CD-Adapco, 2015) was used to generate high quality near wall cells with $y \sim 0.5$.

Both the tanker and tug geometries were locked in all degrees of freedom throughout the analysis. The upstream end of the domain was considered as a velocity inlet, the downstream end as a pressure outlet, the side and bottom surfaces as walls, and the top boundary was also considered as a velocity inlet (Fig. 3). The latter significantly increases the simulation's stability and reduces the simulation time, while maintaining the same degree of accuracy for free-surface simulations compared to a slip wall boundary (CD-Adapco, 2015; Tezdogan et al., 2015).

Fonfach (2010) and Fonfach et al. (2011) used symmetry plane modelling technique for their studies of interaction effects to significantly reduce the computational effort by reducing a large number of cells. A similar approach was also employed in this study with only the Port half of the tanker modelled with the use of a symmetry plane to reduce computational effort. To check the effect of the symmetry plane on the interaction predictions, compatible simulations were carried out using two different domains, one consisting of the complete tanker hull and the other the half tanker hull with the symmetry plane. The maximum difference between the forces and moments on the tug obtained for the two simulation domains were within 0.5% of each other, and this was deemed acceptable for the current study. Therefore, all simulations for the study were conducted with the half tanker hull with the symmetry plane domain. The trimmed cell mesher (CD-Adapco, 2015) was used to generate unstructured, rigid, hexahedral fixed cells within the simulation domain. Cell sizes were refined using volumetric control option in certain areas around the tug boat and the free surface to ascertain a progressively refined grid to capture the complex flow features. All the CFD cases were simulated in double precision mode with the variables of interest converging to four significant figures

Table 2. The y^+ and turbulence model combinations tested for parallel and 30^0 drifted tug operation simulations.

Grid Number	y^+	Turbulence Models used		
		SST	SA	RKE
1	0.1	✓	✓	✓
2	0.5	✓	✓	✓
3	1	✓	✓	✓
4	1.5	✓	✓	✓
5	2	✓	✓	✓
6	5	✓	✓	✓
7	10	✓	✓	✓
8	20	✓	✓	✓
9	30	✓	✓	✓
10	50	✓	✓	✓
11	100	✓	✓	✓

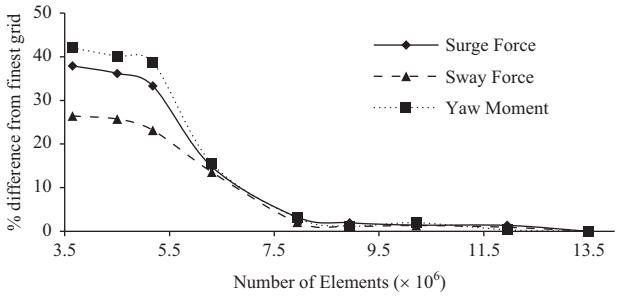

Fig. 4. Percentage (%) difference from the finest 13.5 million elements mesh for the predicted forces and moment, with varying mesh element size.

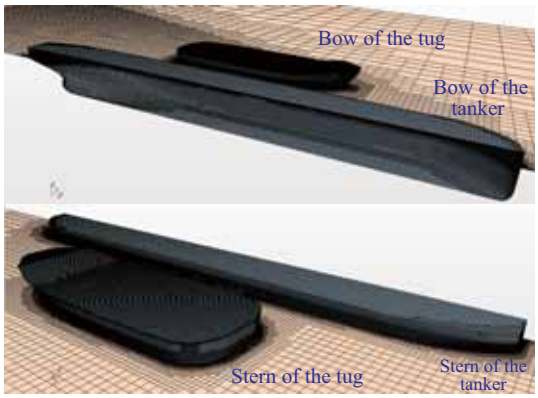

Fig. 5. Selected 8.94 million element mesh grid.

over 50 iterations to mitigate the truncation error. For the CFD simulations, due to the presence of the turbulence stimulator in the experiment, fully turbulent wall treatment model was used. See Gui et al. (2000); Olivieri et al. (2001); Xun et al. (2010); Yoon et al. (2015a); Yoon et al. (2015b) for similar work, and Section 4.2 for additional information on the turbulence stimulators employed. No overset mesh was employed since there was no relative motion between the vessels.

III. VERIFICATION STUDY

The verification conducted consisted of mesh sensitivity, y^+, and turbulence model studies. These are described below.

1. Mesh Sensitivity Study

For the mesh sensitivity study, the tug was kept at the midship region of the tanker ($\Delta X = 0.5$) with zero degree drift angle and lateral separation of $\Delta Y = 1.25$. The surface mesh size was systematically varied, while keeping the SST turbulence model with the y at a constant value of 0.5 to investigate the effect of mesh resolution on the interaction results. Nine meshes were generated by carrying out mesh refinement, especially on the vessel hull surfaces in the pressure interaction region between the vessels and in the forward and aft regions around the vessels. The best mesh was selected by analysing the surge force, sway force, and yaw moment acting on the tug boat and comparing them against those obtained for the mesh consisting of the finest elements as shown in Fig. 4. As seen in the figure, for the 7.9 million element mesh, the forces and moment were within 4% of the finest (13.5 million) mesh, with further refinement causing very little change in convergence. As a conservative measure the 8.94 million element mesh was selected (Fig. 5) for the remainder of the study, which had a maximum deviation of less than 2% from the 13.5 million mesh for both forces and yaw moment. A detailed numerical uncertainty analysis in line with the ITTC (2002a) is also provided in Appendix A to further justify the usage of the selected mesh.

2. y^+ and the Turbulence Model Study

Using the 8.94 million mesh, various combinations of y^+ and turbulence models were tested, as shown in Table 2, at both the parallel and tug at 30 degree drifted operations. When using turbulence models it was important to select models that were suitable for the task at hand as they are optimized for different situations. Three distinct turbulence models i.e., RKE, SST, and SA were investigated in this section along with a y^+ ranging from

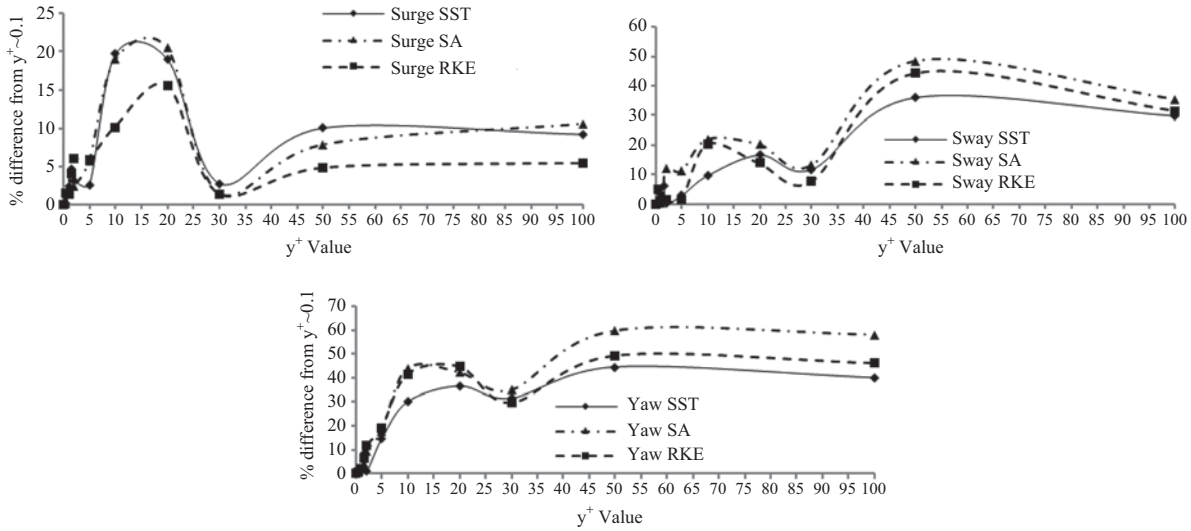

Fig. 6. Percentage (%) difference from the simulation using the smallest y^+ value (0.1) for the predicted surge and sway forces, and yaw moment, with varying y^+ values for parallel tug and tanker operation for the three different turbulence models.

0.1 to 100 to identify the most suitable turbulence model and y^+ combination for ship-tug interaction simulations. All three turbulence models were selected with the all y^+ wall treatment options provided within Star-CCM+®. This enabled the turbulence model to automatically switch between the wall function approach, if the near wall cell lay within the logarithmic region ($y^+ > 30$) or resolving into the viscous sub-layer, if the cells were closer to the surface ($y^+ < 5$). If the value lay within the buffer region ($5 < y^+ < 30$), the wall treatment mathematically blended the linear and logarithmic solutions to predict the wall shear stress.

As seen in Table 2, 33 different cases were evaluated to determine the best combination for two test conditions, i.e., tug parallel, and drifted at 30 degrees to the tanker. The results from the simulations were non-dimensionalised and plotted separately for parallel and drifted operations under surge force, sway force, and yaw moment for evaluation as shown in Fig. 6 and Fig. 7. For the parallel tug operations (Fig. 6), the forces and moment predictions using all three turbulence models when $y^+ < 1$ were found to be within 2.5% of the values obtained for the smallest y^+ of 0.1. However, for $1 < y^+ < 5$, the deviation of the surge forces for all three turbulence models increased to 6%, with the trend continuing until the y^+ approached 30, when the deviation dropped back to around 5% for the RKE turbu-lence model. Further increase in y increased the deviation of the predicted surge forces for all three turbulence models.

Similarly, the percentage difference in the predicted sway forces increased to around 12.25% within the initial y^+ range of 5. Among the three turbulence models, the SA model showed this largest deviation of up to $y^+ \sim 5$, which was 12.25%, while the SST and RKE turbulence models showed maximum deviations of 6.19% and 4.98% respectively. When the y^+ further increased, the % difference of the surge and sway forces decreased as y^+ approached 30, with the maximum difference found at 9.31%, for the sway force predicted by the RKE model. This sudden decrease was possibly due to the turbulence models switching automatically to the wall function as the y^+ moved from the buffer region to the logarithmic region. Beyond a y^+ of around 35, the results significantly deteriorated.

It is evident that when the near wall cell lies within the buffer region ($5 < y^+ < 30$), all turbulence models showed larger % deviations. This agrees with the finding presented by Salim and Cheah (2009), that when the first node is within the buffer region, neither the wall function approach nor the wall modelling approach can provide results with sufficient accuracy. Thus, the results obtained for the tug and tanker parallel operations confirm that the least deviated results are obtained when $y^+ < 1$, i.e., when the sub layer is resolved, although a $y^+ \sim 30$ provided reasonable accuracy through the use of the wall function. The buffer region of $5 < y^+ < 30$ did not provide satisfactory results with any of the three turbulence models used in this study.

The yaw moment displayed a similar pattern to surge and sway forces, i.e., for $y^+ < 1$ the maximum difference was 2.25% for the SA turbulence model, and this increased to 18.9% when y^+ reached 5. Further increase in the y^+ value increased the deviation beyond 30% for all three turbulence models, with a temporary dip back to 30% at $y^+ \sim 30$ due to the models switching to the wall function as discussed above. Thus, it's clear that only for the $y^+ < 1$ condition do the surge force, sway force and yaw moment predictions fall within acceptable margins. The least deviation within that $y^+ < 1$ region was using the SST turbulence model, while the SA model gave the largest error. Star-CCM+® guidance on the use of turbulence models states that the SA model is best for mild separation flows such as flow past a wing (CD-Adapco, 2015). However, the flow past the transom stern of the tug model resulted in severe separation due to the blunt body at the trailing edge creating wakes and disturbed flow. In the past the authors have confirmed (Jayarathne et al., 2014) that for a transom stern tug operating near a tanker, accurate

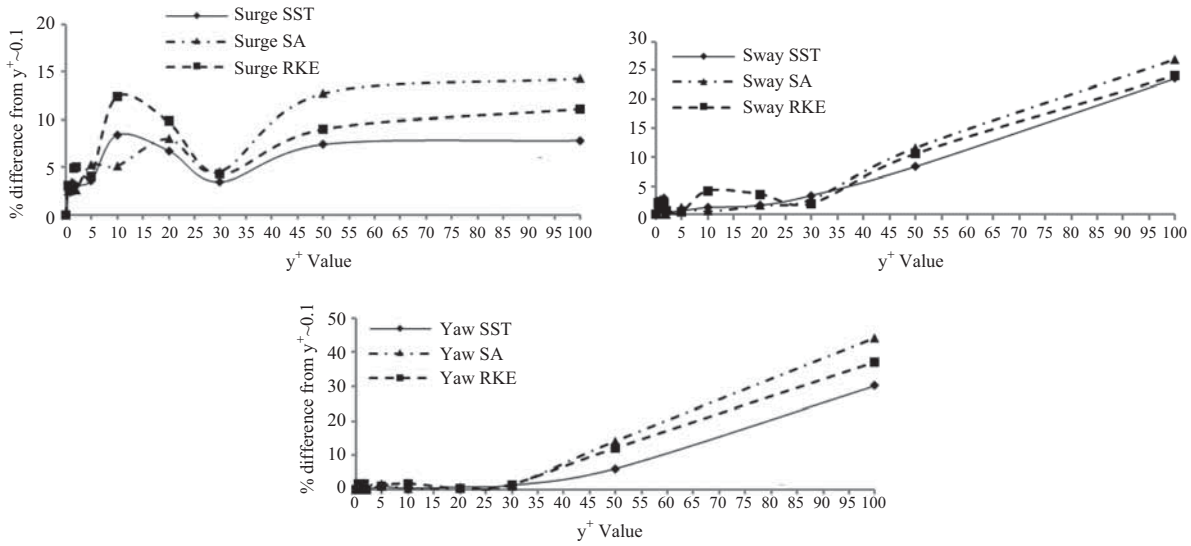

Fig. 7. Percentage (%) difference from the simulation using the smallest (0.1) y^+ value for the predicted surge and sway forces and yaw moment, with varying y^+ value for 30^0 drifted tug and tanker operation for the three different turbulence models.

flow separation prediction is one of the crucial factors for determining interaction effects.

Fig. 7 illustrates the forces and moment predictions when the tug was drifted by 30 degrees to the tanker. As seen in the plots, the surge forces for $y^+ < 1$ show a maximum % deviation of 2.87% from the results for a grid with a y^+ of 0.1, which was for the SA turbulence model. As the y^+ value was increased within the viscous sub-layer, i.e., $1 < y^+ < 5$, the maximum % deviations for the three models increased, with the SA model being the highest again at 5.31%. For $5 < y^+ < 30$, i.e., within the buffer region, the % deviation increased, with the maximum being 12.43% for the RKE model. As per the recommendation by Star-CCM+® (CD-Adapco, 2015), the RKE two-layer formulation works with either Low-Reynolds number type grids, i.e., $y^+ \sim 1$ or wall-function type grids, i.e., y^+ around 30. Thus, when the y^+ is within the buffer region, the deviation was larger than those experienced in other regions. At $y^+ \sim 30$, the % deviations were significantly reduced to around 5%, which then rapidly increased as the y increased to 100.

The sway force prediction differences were similar to the surge force differences for all three turbulence models showing a maximum of 2.72% for the SA model when $1< y^+$. An increased y^+ value amplified the deviation for all turbulence models, with the expected dip at $y^+ \sim 30$. Yaw moment differences were less distinguishable for smaller y^+ values. However, the maximum % difference of moments was found in the RKE model for $1 < y^+$, which was 1.56%. While the deviation increased within the logarithmic region (i.e., $y^+ > 30$), the differences increased significantly beyond 30% for all three turbulence models.

Among the three turbulence models tested, the SST model showed the least deviation in most of the cases, especially when considering the sway forces and when the tug was drifted creating complicated flow behaviour with flow separations and circulations. In addition, for all models the least % deviations were experienced when $y^+ < 1$. Therefore, the SST turbulence model with a $y^+ \sim 1$ was selected to proceed further in this study. This ensured the results were consistent with the equations solved into the viscous sub layer to predict any adverse pressure gradient and flow separations. The wall function model did not show sufficient accuracy when the y was within the buffer region (i.e., $5 < y^+ < 30$).

IV. VALIDATION STUDY

Keeping the verified simulation model as a base model, a series of compatible model scale numerical simulations and experimental investigations were carried out in order to compare the CFD simulation results with the experimental results.

1. Numerical (CFD) Simulations

Using the same model scale tug and tanker used for the verification study, a new series of simulations were carried out for different ΔX and ΔY (see Eqs. (4) and (5)) values and different tug drift angles with the SST turbulence model and $y^+ \sim 1$. Two flow velocities were used for the study, i.e., at model scale speeds of 0.41 m/s and 0.62 m/s.

The selected cases for the study are given in Table 3, with each case replicated within the CFD simulations and the experimental program. Due to limitations in the experimental arrangement, at a tug drift angle of 8.4 degrees it was not possible to place the tug at a ΔY separation of 1.34, as it would collide with the Drag-On support pillars (see Fig. 9 and Appendix B) used to tow the models. Similarly for the 16.8 degrees drift angle it was only possible to have a ΔY separation of 1.09 as ΔY separations of 1.24 and 1.34 coincided with the Drag-On support pillars.

2. Experimental Investigation

In order to compare the results generated through CFD,

Table 3. Cases investigated for the CFD and experimental comparison study.

Simulation Case Number	Tug Drift Angle θ (degrees)	ΔX (non-dimensionalised)	ΔY (non-dimensionalised)
1	0	0.6	1.09
2	0	0.6	1.24
3	0	0.6	1.34
4	0	1.0	1.09
5	0	1.0	1.24
6	0	1.0	1.34
7	0	1.2	1.09
8	0	1.2	1.24
9	0	1.2	1.34
10	8.4	0.6	1.09
11	8.4	0.6	1.24
12	8.4	1.0	1.09
13	8.4	1.0	1.24
14	8.4	1.2	1.09
15	8.4	1.2	1.24
16	16.8	0.6	1.09
17	16.8	1.0	1.09
18	16.8	1.2	1.09

(a) (b)

Fig. 8. (a) Experimental setup for interaction between vessels in AMC's Model Test Basin and (b) Turbulence simulators used on the models: left image wire on tanker model and right image studs on tug model.

corresponding cases were replicated through captive model experiments in AMC's 35 m (length) × 12 m (width) × 1.0 m (depth) model test basin shown in Fig. 8.

The scaled tanker and tug models were fixed in all degrees of freedom during the study. The tanker model was attached without any strain gauges or sliders below the Drag-On connection box, which was used to guide the models. However, the tug model was attached on to the Drag-On connection box using two strain gauges as shown in Fig. 9, to measure the surge and sway forces and to calculate the yaw moment. Experiments were conducted at the fully loaded drafts of both hulls, with all cases tested for two different speeds of 0.41 m/s and 0.62 m/s in model scale (see Table 4). Both models were attached together to the Drag-On, thus moving forward at the same speed with no relative motion between them. The models were fitted with turbulence stimulators in the form of a wire for the tanker model and studs for the tug model to generate a fully turbulent boundary layer along the hull of the vessels. Locations of the studs

Table 4. Speed regimes tested during validation study.

Speed of vessels			Froude Number based on	
Model Scale (m/s)	Full Scale (m/s)	Full Scale (Knot)	Tug Length	Tanker Length
0.41	1.74	3.4	0.10	0.07
0.62	2.62	5.1	0.15	0.10

Table 5. Results analysis groups.

Drift Angle (Deg)	Group Number	Speed (m/s)	Cases from Table 3
0	1	0.41	1 to 9
0	2	0.62	1 to 9
8.4	3	0.41	10 to 15
8.4	4	0.62	10 to 15
16.8	5	0.41	16 to 18
16.8	6	0.62	16 to 18

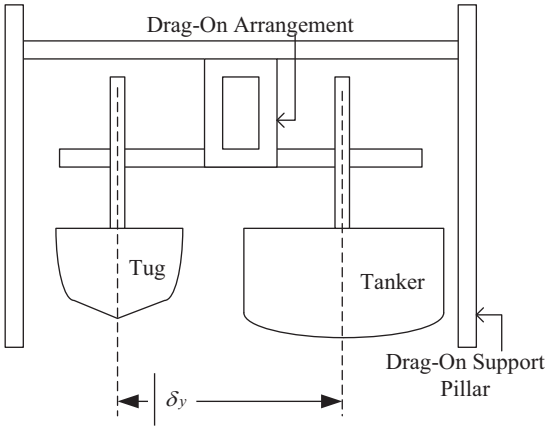

Fig. 9. Schematic of the experimental setup in AMC's Model Test Basin. Additional pictures and sketches of the Drag-On are given in Appendix B.

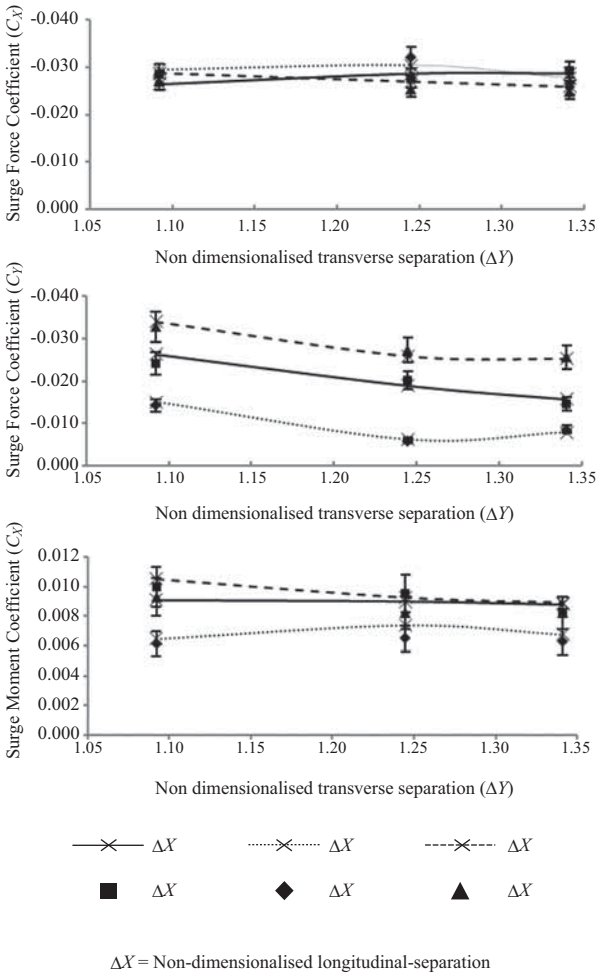

ΔX = Non-dimensionalised longitudinal-separation

Fig. 10. CFD and experimental comparison of surge force, sway force, and yaw moment coefficients acting on the tug when parallel to the tanker and moving forward at a common speed of 0.41 m/s (Group 1).

were calculated based on the ITTC (2011) guidelines and are shown for the two models in Fig. 8(b).

V. DISCUSSION

The surge force, sway force, and yaw moment results obtained from the 36 CFD simulations and their equivalent 36 experimental runs were plotted in six different groups to ease the analysis, as outlined in Table 5. The uncertainty analysis conducted in accordance with ITTC (2002b) for the experimental measurements are presented in Appendix A.

1. Parallel Operation-Drift Angle of 0 Degrees (Groups 1 and 2)

Fig. 10 shows the results for the surge force, sway force, and yaw moment coefficients for the cases in Group 1, when the hulls were parallel and at a forward speed of 0.41 m/s.

The differences between the CFD and experimental results lay well within the uncertainty margins of the experiments. The maximum differences between CFD and experimental surge force, sway force, and yaw moment were found to be 7.7%, 8.8%, and 13.4% respectively. Furthermore, when comparing the CFD and experimental flow behaviour in Fig. 11, it was evident that the free surface between the vessels and around the stern of the tug for the CFD and experimental work show similar flow behaviour, including wave intersection between the vessels.

Fig. 12 shows the three coefficients for Group 2, i.e., at the relative positions as in Group 1 but at a 0.62 m/s forward speed. At 0.62 m/s, the difference between CFD and experimental surge force, sway force, and yaw moment were 9.9%, 11.3% and 13.2% respectively. These differences were within the experimental uncertainty margin and the trends of the surge and sway forces were similar to the plots at the speed of 0.41 m/s. However, the maximum yaw moments were experienced at different longitudinal separations, at $\Delta X = 1.2$ for 0.41 m/s and at $\Delta X = 0.6$ for 0.62 m/s. It is noted that when the flow speed increased, the tanker's bow wave was more prominent and its effect on the tug increased. Thus, yaw moment was larger at $\Delta X = 0.6$ at a speed of 0.62 m/s, in comparison to the $\Delta X = 1.2$. In contrast to this, for both speeds the least yaw moments were experienced when the tug was around the midship region of the tanker (i.e., $\Delta X = 1.0$), similar to the findings of Dand (1975), which discussed the interaction effects acting on a tug when it overtakes a larger ship.

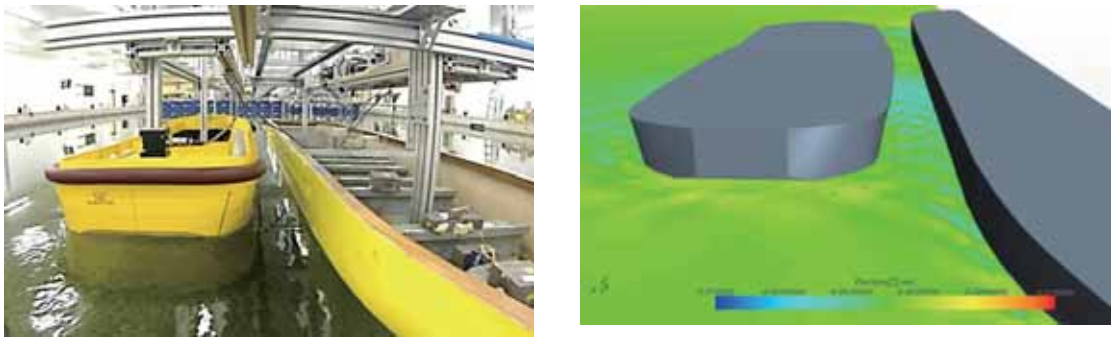

Fig. 11. Experimental and CFD free surface at a common forward speed of 0.41 m/s at ΔX = 1.2, ΔY = 1.09, and θ = 0 degree.

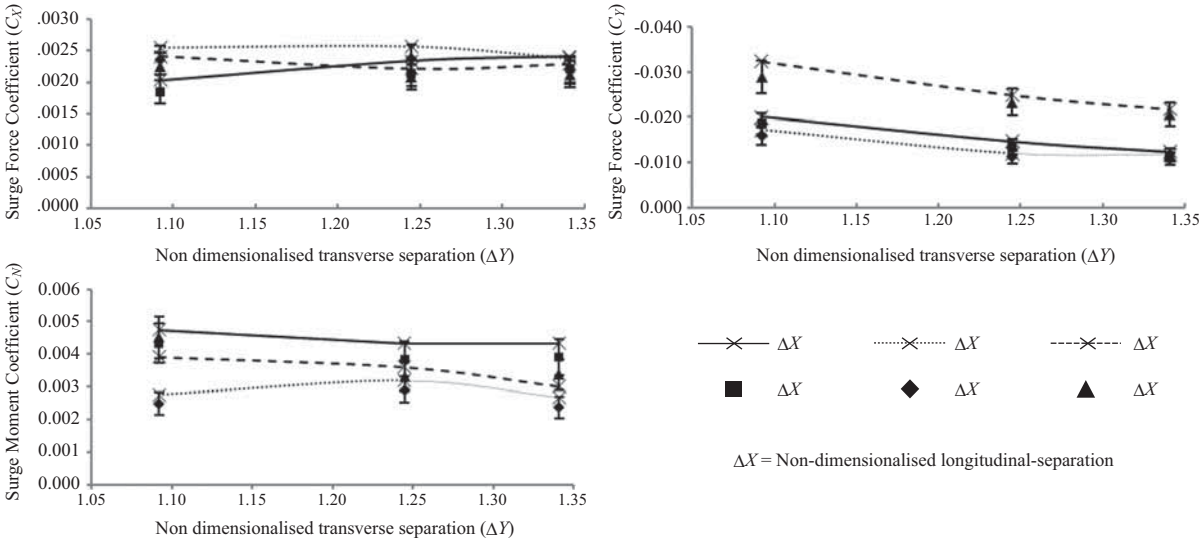

Fig. 12. CFD and experimental comparison of surge force, sway force, and yaw moment coefficients acting on the tug when parallel to the tanker and moving forward at a common speed of 0.62 m/s (Group 2).

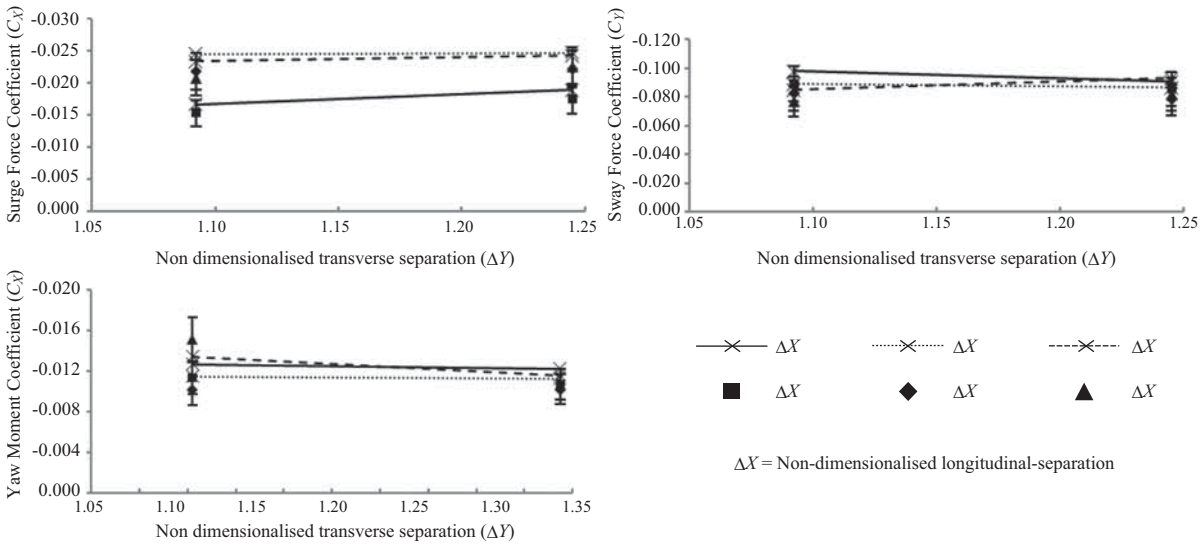

Fig. 13. CFD and experimental comparison of surge force, sway force, and yaw moment coefficients acting on the tug when drifted 8.4 degrees to the tanker and moving forward at a common speed of 0.41 m/s (Group 3).

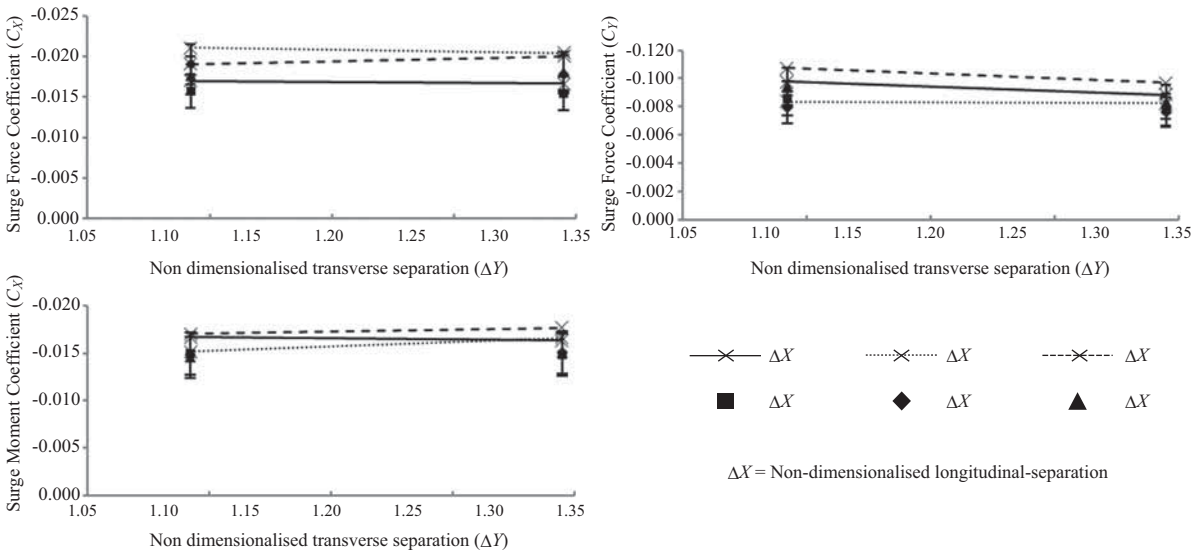

Fig. 14. CFD and experimental comparison of surge force coefficient, sway force coefficient, and yaw moment coefficient acting on the tug when drifted 8.4 degrees to the tanker and moving forward at a common speed of 0.62 m/s (Group 4).

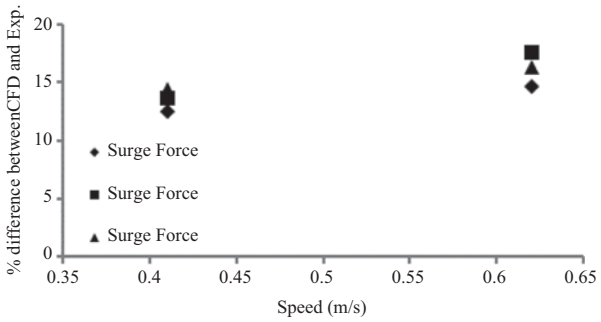

Fig. 15. Percentage (%) difference between the CFD simulations and Experimental investigation results for tug with 8.4 degrees drift angle at 0.41 m/s and 0.62 m/s speeds.

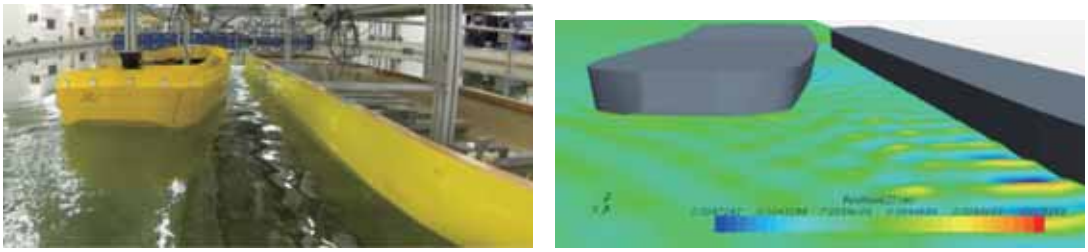

Fig. 16. Experimental and CFD free surface at a common forward speed of 0.41 m/s at ΔX = 1.0, ΔY = 1.01, and θ = 8.4 degrees.

2. Drift Angle of 8.4 Degrees (Groups 3 and 4)

The results for Group 3 and Group 4, which represents the 0.41 m/s and 0.62 m/s speeds respectively at a tug drift angle of 8.4 degrees are illustrated in Fig. 13 and Fig. 14 respectively. As seen in Fig. 13, the difference between the CFD and the experimental results were 12.5% for the surge force coefficient, 13.6% for the sway force coefficient, and 14.4% for the yaw moment coefficient, with all CFD predictions lying within the experimental uncertainties explained in Appendix A.

As illustrated in Fig. 14, % differences between CFD and experimental results increased when the speed of the vessels was increased to 0.62 m/s in the Group 4 cases. These are shown in Fig. 15, with the increased % differences being: surge force coefficient 14.7%, sway force coefficient 16.3%, and yaw moment coefficient 17.6%. Thus at 0.62 m/s, the CFD predictions were slightly beyond the experimental uncertainty margin by 1.4%, 0.5% and 2.5% respectively. Simonsen et al. (2011) also ex-

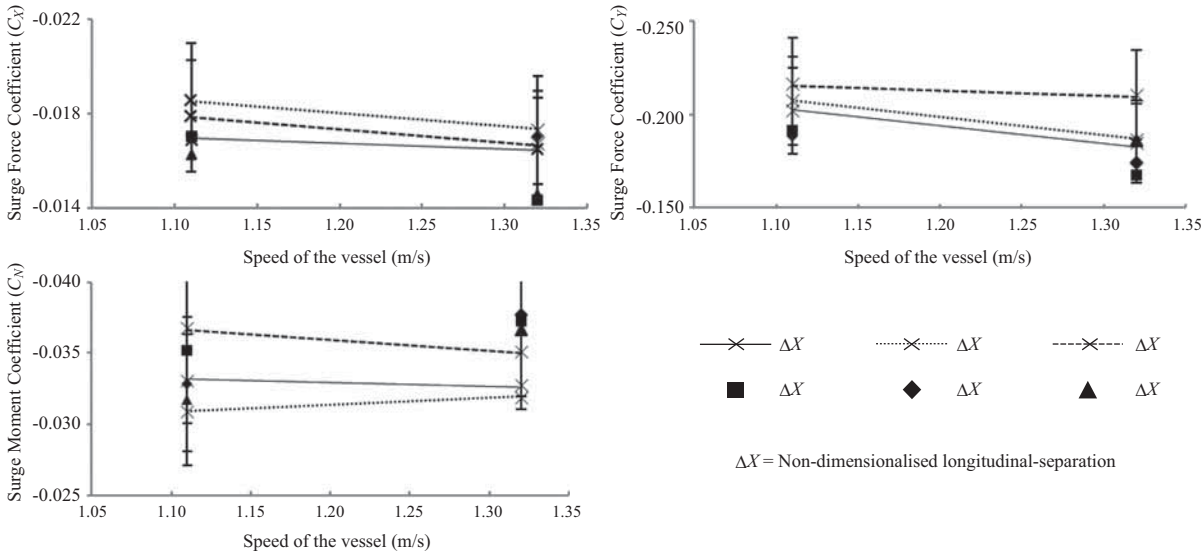

Fig. 17. CFD and experimental comparison of surge force coefficient, sway force coefficient, and yaw moment coefficient acting on the tug when drifted at 16.8 degrees to the tanker and moving forward at common speeds of 0.41 m/s and 0.62 m/s, lateral separation ΔY of 1.09, and varying longitudinal separations ΔX (Groups 5 and 6).

perienced a similar mismatch between CFD and experimental results at larger drift angles, concluding that the CFD had good qualitative agreement with the experimental results. Yet, if the expected precision limit of the results is high, the causes for these differences have to be thoroughly investigated. Though the differences in the results were more than the experimental uncertainty calculated in accordance with that presented in Appendix A, the trend and the flow behaviour look similar in both cases.

Fig. 16 shows the comparison of the flow behaviour predicted by the CFD and that seen during the equivalent experimental run.

3. Drift Angle of 16.8 Degrees (Groups 5 and 6)

Finally the results for Group 5 and Group 6 for the tug drifted by 16.8 degrees were analysed. Due to the limitations of the towing rig used for the experiments, only one transverse separation ($\Delta Y = 1.09$) was considered for this drift angle. However, longitudinal location was changed to similar locations ($\Delta X = 0.6$, 1.0, 1.2) as with Groups 1 to 4, and the tests were conducted for similar common speeds of 0.41 m/s and 0.62 m/s. The surge force, sway force, and yaw moment coefficient results for the two groups were plotted against the common speed in Fig. 17.

At this drift angle, the differences between the CFD and experimental results at 0.41 m/s for the surge force and sway force coefficients were 9.8% and 12.6% respectively, while the difference for the yaw moment coefficient was 14.4%. As the speed was increased to 0.62 m/s the differences between the CFD predictions and the experimental results increased to 13.8%, 12.9% and 15.8% respectively. Similar to the Group 4 results discussed earlier, they were marginally beyond experimental uncertainty by 0.6%, 1.5% and 1.3% respectively.

Thus, it is seen that with the increasing Froude number, CFD prediction showed a slight deviation away from the experimental results. However, doubling the drift angle from 8.4 to 16.8 degrees showed a little change in the difference between the CFD and the experimental results. Consequently, this error was deemed as being dependent on the Froude number rather than the drift angle. Nevertheless, it is necessary to investigate similar operations with larger Froude numbers to identify the real cause for this deviation. However, the current study is limited to investigating interaction effects on tugs when assisting ships entering or leaving ports, where the tugs operate within their lower speed range, typically around 3 to 6 knots, and thus at smaller Froude numbers, as speeds beyond 6 knots become too high for effective tug assistance (Hensen, 2003). Therefore, the verified CFD parameters within this study were deemed competent for predicting the interaction effects of the tug-ship interaction scenarios considered at typical tug assist operational speeds.

VI. CONCLUSION

This paper outlines a comparative numerical and experimental study conducted to investigate the suitability of RANS based CFD simulations for predicting the interaction effects acting on a tug during ship assist operations. It includes investigating the selection of appropriate turbulence models and boundary layer modelling on the simulation results. Three distinct turbulence models (i.e., RKE, SST, and SA) and y ranging from 0.1 to 100 were included within this interaction prediction study to identify the most appropriate turbulence model and y^+ combination. The uncertainties of EFD for parallel vessel operations were quantified using ITTC (2002b) at 7%, 9.4%, and 7% for surge force, sway force, and yaw moment respectively.

It was shown that for $y^+ \leq 1$ the SST turbulence model offered good agreement with the experimental measurements for both the parallel and drifted tug manoeuvre test cases at the speed

range tested (i.e., Froude number 0.10 to 0.15 based on tug's length). For the cases within the $1 < y^+ < 5$ range, the RKE results closely followed the SST results with a maximum difference of around 2%. Within this region, the SA turbulence model showed the largest discrepancy among the three turbulence models, at around 12%. This confirms that the SA model is best for mild separation flows, such as flow past a wing at low angle of attack, whereas for tugs, with a submerged transom stern, a highly separated flow is created resulting instability and accuracy issues in the numerical modelling.

The region $5 < y^+ < 30$ does not provide good results with any of the three turbulence models used in this study due to inaccurate blending of the linear and logarithmic solutions to predict the wall shear stress. If the computational resources are limited, then a y^+ at 30 can provide a reasonable result with the wall function model. A $y^+ > 30$ was found to be inadequate for the investigation of interaction effects due to the large result deviations found in this study. When the tug was drifted to higher angles, i.e., 8.4 degrees and 16.8 degrees, the CFD predictions with the SST turbulence model and $y^+ \leq 1$ were above the EFD uncertainties maximum by 2.5%. Furthermore, it was found that the major cause for the increased discrepancies was the increased Froude number, and not the drift angle. However, for ship assist operations the Froude numbers will be relatively low due to operational limitations on the speeds and thus the selected turbulence model and y combination were found to be acceptable for interaction effect studies.

Based on this, a use of SST turbulence model with smaller y^+ values is planned to further extend this study. This will involve simulations of more tug and tanker combinations by increasing the tug's drift angle up to 90 degrees and changing its location throughout the tanker length and beyond to quantify the interaction effects under different scenarios and identify safe tug operational envelopes when operating in proximity to a large vessel. In addition, the current models will form the basis to develop full scale simulation models to investigate tugs and tankers having relative motion, to identify the interaction effects when a tug is approaching a tanker underway during rope handling operations.

VII. NOMENCLATURE

B_s	Breadth of the tanker (m)
B_t	Breadth of the tug (m)
CFD	Computational Fluid Dynamics
C_N	Yaw moment coefficient
C_X	Surge force coefficient
C_Y	Sway force coefficient
EFD	Experimental Fluid Dynamics
F_r	Froude Number (Tug Length), $Fr = u / \sqrt{gL_t}$
g	Acceleration due to gravity (9.81 m/s^2)
RKE	Realizable Two Layer k-ε turbulence model
L_s	Length waterline of the tanker (m)
L_t	Length waterline of the tug (m)
N	Yaw moment acting on tug (Nm)
RANS	Reynolds Averaged Navier-Stokes
SA	Spalart-Allmaras turbulence model
SST	Shear Stress Transport turbulence model
u	Fluid flow velocity (m/s)
X	Surge force acting on tug (N)
Y	Sway force acting on tug (N)
y^+	Non-dimensional wall distance of first inflation layer
ΔX	Non-dimensionalised longitudinal-distance between vessels
δx	Longitudinal distance between vessels (m)
ΔY	Non-dimensionalised transverse distance between vessels
δy	Transverse distance between vessels (m)
ρ	Density of water (kg/m^3)
∇_s	Volumetric displacement of the tanker (m^3)
∇_t	Volumetric displacement of the tug (m^3)

ACKNOWLEDGEMENTS

Authors would like to thank AMC model test basin staff for their valuable support during the experiments.

APPENDIX A

EXPERIMENTAL AND NUMERICAL UNCERTAINTY ANALYSIS

A1. Experimental Uncertainty Analysis

This section provides detailed calculations of the uncertainty analysis for the captive model scale experimental work carried out in AMC's model test basin. The uncertainty analysis procedure given in ITTC (2002b) was followed within this study.

In according with ITTC (2002b), the total uncertainty limit of a model experiment is divided into bias and precision limits. This section discusses the estimation of the total uncertainties for single and multiple ship model experiments for ship interaction studies. Based on the total uncertainty limit, the percentage of uncertainty was calculated. The calculations given here is an example, dealing with the surge force calculation for one of the cases investigated, where both vessels are parallel to each other (i.e., $\theta = 0$ degree) and travelling at a forward speed of 0.41 m/s with the tug located at $\Delta X = 1.0$ and $\Delta Y = 1.09$.

The surge, sway and yaw coefficients were calculated based on the following formulae (Sutulo and Soares, 2009; Fonfach et al., 2011; Simonsen et al., 2011):

$$C_X = \frac{2X}{u^2 \nabla_t^{1/3} \nabla_s^{1/3} \rho} \tag{A1}$$

$$C_Y = \frac{2Y}{u^2 \nabla_t^{1/3} \nabla_s^{1/3} \rho} \tag{A2}$$

$$C_N = \frac{2N}{u^2 \nabla_t^{1/3} \nabla_s^{1/3} L_t \rho} \tag{A3}$$

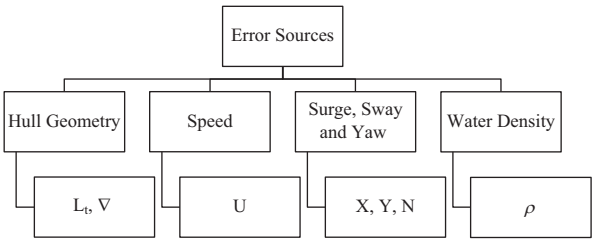

Fig. A1. Error sources used for the uncertainty analysis.

For the surge and sway force coefficients, the following bias limits were considered:

(1) Surge force and sway force (B_X, B_Y);
(2) Speed (B_U);
(3) Volume of displacement (B_{∇_t}); and
(4) Density measurement (B_ρ).

For the yaw moment coefficient, the bias limits were as follows:

(1) Sway force forward and aft (B_Y);
(2) Speed (B_U);
(3) Volume of displacement (B_{∇_t});
(4) Density measurement (B_ρ); and
(5) Tug length (B_{L_t}).

Error sources creating the bias limits are shown in the Fig. A1. Uncertainty sources that were smaller than 25% of the largest sources were neglected. Hence, acceleration due to gravity was not included in the calculation.

The total experimental uncertainty is given by the root sum square of the uncertainties of the total bias and precision limits,

$$\sigma_T^{\,2} = B_T^{\,2} + P_T^{\,2} \tag{A4}$$

where,

σ_T = *total experimental uncertainty*

B_T = *total bias limit*

P_T = *total precision limit*

Surge Force (Example Calculation)

For the surge force coefficient, Eq. (A4) is modified as,

$$\sigma_T^{\,2} = B_T^{\,2} + P_T^{\,2} \tag{A4}$$

where,

σ_T = *total experimental uncertainty for surge force coefficient*

B_T = *total bias limit for surge force coefficient* (A6)

P_T = *total precision limit for surge force coefficient*

where,

$$\frac{\partial C_x}{\partial X} = \frac{2X}{U^2 \nabla_t^{\,1/3} \nabla_s^{\,1/3} \rho} \tag{A7}$$

$$\frac{\partial C_x}{\partial U} = \frac{-4X}{U^3 \nabla_t^{\,1/3} \nabla_s^{\,1/3} \rho} \tag{A8}$$

$$\frac{\partial C_x}{\partial \rho} = \frac{-2X}{U^2 \nabla_t^{\,1/3} \nabla_s^{\,1/3} \rho^2} \tag{A9}$$

$$\frac{\partial C_x}{\partial \nabla_t} = \frac{-2X}{3U^2 \nabla_t^{\,1/3} \nabla_s^{\,1/3} \rho^2} \tag{A10}$$

Calculation for B_X

Three major factors are found within B_X; i.e., as the bias due to the calibration weight (B_{X1}), bias from the calibration factor (B_{X2}) and bias due to the load cell misalignment (B_{X3}), which were considered here.

Bias Due to the Calibration Weight (B_{X1})

Tolerance of the standard calibration weights used for the experiments was ±0.005%. Measured surge force at the selected case was 0.8370N.

$$B_{X1} = 0.005 \times 0.8370N = 0.004185N.$$

Bias from the Calibration Factor (B_{X2})

Maximum error found in a series of calibrations done during the experiments was 2.44 g. Load cell error including hysteresis and non-linearity was 0.4%. Therefore, the maximum expected bias is,

$$B_{X2} = \left(0.005 \times 9.81 \div 1000\right)\left(1 + 0.114\right)N$$

$$B_{X2} = 0.02403N.$$

Bias Due to the Load Cell Misalignment (B_{X3})

This error was manifested due to the load cell misalignment during calibration and testing. The maximum bias limit expected was ±0.5 degrees and it will affect the resistance measurement as follows,

$$B_{X3} = X - \left(\cos 0.05X\right)$$

$$B_{X3} = 0.8370 - \left(\cos 0.5\ 0.8370\right)$$

$$B_{X3} = 0.000032N.$$

Total Bias Limit on Force Measurement (B_X)

The total bias limit on the surge force is obtained by the root sum square of the components considered above, i.e.,

$$B_X^2 = B_{X1}^2 + B_{X2}^2 + B_{X3}^2$$

$$B_X = 0.2439N.$$

Calculation for B_U

Bias limit for the speed was calculated using the speed displayed on the carriage display and the real speed expected without error. The speed voltage calibration factor was 0.5 m/s/V and the voltage reading at the average speed was 0.825535 V. Therefore, the expected speed was 0.4127 m/s. However the speed displayed on the model test basin display was 0.4102 m/s. Therefore, the expected bias limit is obtained as the difference of these speeds.

$$B_U = 0.0025 \text{ m/s}$$

Calculation for B_U

In order to calculate bias limit for the density; three factors are considered, i.e., the bias limit of the temperature measurements (B_t), bias limit for the density calibration ($B_{\rho 1}$), and bias limit for the data reduction ($B_{\rho 2}$).

Bias Limit of the Temperature Measurements (B_t)

Since the temperature is involved in density calculation, the bias limit of the temperature measurements is required. Accuracy of the thermometer used for temperature measurements was ±0.3 degrees within -5 to 50 degrees. The temperature reading for the selected case was 17 degrees. Therefore, the bias limit for the temperature was obtained as,

$$B_t = 0.3$$

Bias Limit for the Density Calibration ($B_{\rho 1}$)

In order to calculate the bias limit for the density measurement (B_ρ), the following formulae (ITTC, 2002b) was used,

$$\rho = 1000.1 + 0.0552t - 0.0077t^2 + 0.0004t^3 \qquad \text{(A11)}$$

$$\left|\frac{\partial \rho}{\partial t}\right| = \left|0.0552 - 0.0154t + 0.00012t^2\right| \qquad \text{(A12)}$$

For $t = 17^0$ and $B_t = 0.3$

$$B\_\rho 1 = 0.052 \text{ kg/m}^3.$$

Bias Limit for the Data Reduction ($B_{\rho 1}$)

When the nominal temperature was substituted in to Eq. (A11), the density ρ was obtained as 1000.7783 kg/m^3.

However from the density tables, the density was found as 998.7780 kg/m^3 for a temperature of 17 degrees.

Therefore the difference in density is 0.232 kg/m^3.

Hence,

$$B_{\rho 2} = 2.0003 \text{ kg/m}^3.$$

Total Bias Limit for the Density (B_ρ)

$$B_\rho^2 = B_{\rho 1}^2 + B_{\rho 2}^2$$

$$B_\rho = 2.001 \text{ kg/m}^3. \qquad \text{(A13)}$$

Calculation for B_{∇_t}

The tug's volume of displacement (∇_t) was calculated by dividing the mass (m) of the model measured using a floor scale by the density (ρ)of the water in the model test basin. Hence the bias limit of the density and mass should be included in the bias limit for the volume of displacement.

$$\nabla_t = \frac{m}{\rho} \qquad \text{(A14)}$$

$$B_{\nabla_t}{}^2 = \left(\frac{\partial \nabla_t}{\partial m} B_m\right)^2 + \left(\frac{\partial \nabla_t}{\partial \rho} B_\rho\right)^2 \qquad \text{(A15)}$$

where,

$$\frac{\partial \nabla_t}{\partial m} = \frac{-m}{\rho} \qquad \text{(A16)}$$

$$\frac{\partial \nabla_t}{\partial \rho} = \frac{-m}{\rho^2} \qquad \text{(A17)}$$

$B_m = 0.05$ kg for the floor scale used

$B_\rho = 2.001 \text{ kg/m}^3$ as calculated before

$$\textit{nominal 'm'} = 79.55 \text{ kg}$$

$$\textit{nominal '}\rho\textit{'} = 998.778 \text{ kg/m}^3$$

Therefore,

$$B_{\nabla_t} = 0.00398 \text{ m}^3$$

Calculation for $B_{T_{cx}}$

Using the nominal values calculate above, the partial differentials for each bias limit is obtained from Eqs. (A7)-(A10).

Using,

$$X = 0.837N$$

$$U = 0.4102675 \text{ m/s}$$

$$\nabla_t = 0.07964 \text{ m}^3$$

$$\nabla_s = 0.531 \text{ m}^3$$

$$\rho = 997.778 \text{ kg/m}^3$$

The partial difference become,

$$\frac{\partial C_x}{\partial X} = 0.0341$$

$$\frac{\partial C_x}{\partial U} = 0.1393$$

$$\frac{\partial C_x}{\partial \rho} = 2.8615 \times 10^{-5}$$

$$\frac{\partial C_x}{\partial \nabla_t} = 0.1196$$

Thus, from the Eq. (A6) we get the total bias limit for the surge force coefficient as,

$$B_{T_{cx}} = 0.001022$$

Calculation for $P_{T_{cx}}$

In order to establish the precision limit, the standard deviation of the number of tests with the model removed and reinstalled between two runs must be determined. Hence six different runs with the same speed and location settings were conducted to measure the forces acting on the tug.

The precision limit for multiple tests $P(M)$ and precision limit for a single run $P(S)$ are calculated according to (ITTC, 2002b) as,

$$P(M) = \frac{k.SDev}{\sqrt{M}} \quad \text{(A18)}$$

$$P(S) = k.SDev \quad \text{(A19)}$$

where;

K = 2 according to the methodology

$SDev$ = standard deviation established by multiple runs

Table A1. Experimental Uncertainty percentages calculated for the interaction effects at three drift angles.

Interaction Effect	0 degree Drift Angle	8.4 degrees Drift Angle	16.8 degrees Drift Angle
Surge Force	7.0%	13.3%	13.2%
Sway Force	9.4%	15.8%	11.4%
Yaw Moment	7.0%	15.1%	14.5%

Table A2. Calculated iterative uncertainties for the fine (G_1), medium (G_2) and coarse (G_3) grids.

Grid label	No of cells	Iterative Uncertainties		
		Surge	Sway	Yaw
G_1	8.94 M	0.07% *EFD*	0.15% *EFD*	0.21% *EFD*
G_2	6.31 M	0.09% *EFD*	0.15% *EFD*	0.22% *EFD*
G_3	4.50 M	0.09% *EFD*	0.18% *EFD*	0.20% *EFD*

M = number of runs

Using Eqs. (A18) and (A19) we get,

$$P(M) = 0.00069$$

$$P(S) = 0.00169$$

Therefore, the total surge force uncertainty using Eq. (A5) is established as,

$$\sigma_{T_{cx}} = 7\%$$

Sway Force and Yaw Moment

In order to establish the uncertainty limit for the sway force and yaw moment, similar calculations were conducted giving,

$$\sigma_{T_{cy}} = 9.4\%$$

$$\sigma_{T_{cn}} = 7\%$$

All these calculations were repeated for the different drift angles and different speeds of the tug boat, enabling the calculation of error bars for the result plots as shown in Table A1.

A2. Numerical Uncertainty Analysis

Surge force, sway force, and yaw moment acting on the tug boat using three selected CFD grids (Table A2) were used to investigate the numerical accuracy of the CFD solutions in accordance with ITTC (2002a) procedures explained in the following section. Once the numerical accuracy was investigated, y^+ and turbulence model combinations were varied to observe their effects on the computational results.

In order to investigate numerical accuracy in the CFD solu-

Table A3. Results obtained from the grid convergence study for the surge force (X), sway force (Y), and yaw moment (N) as a percentage of finest grid results ($\%G_1$).

Parameter	$\delta_G^*(\%G_1)$	$U_G(\%G_1)$	$U_{G_C}(\%G_1)$
X	0.054071	-5.817	-0.034
Y	0.000002	-0.587	-0.292
N	0.060046	2.731	1.321

Note: δ_G^* is the estimated grid convergence error, U_G is the grid convergence uncertainty and δ_{G_C} is the corrected grid convergence uncertainty.

Table A4. Results obtained from the time step convergence study for surge force (X), sway force (Y), and yaw moment (N) as a percentage of finest grid results ($\%G_1$).

Parameter	$\delta_T^*(\%G_1)$	$U_T(\%G_1)$	$U_{T_C}(\%G_1)$
X	0.005580	-1.639	-0.519
Y	0.001667	-4.617	-1.847
N	0.000004	0.176	0.086

Note: δ_T^* is the estimated grid convergence error, U_T is the grid convergence uncertainty and δ_{T_C} is the corrected grid convergence uncertainty.

Table A5. Verification uncertainty values (U_V) as a percentage of the EFD for CFD generated surge force (X), sway force (Y), and yaw moment (N) results and corrected surge force (X_C), sway force (Y_C), and yaw moment (N_C) results.

Parameter	U_{SN} (%EFD)	U_D (%EFD)	U_V (%EFD)	$\%\lvert E\rvert$
X	-5.99	7.0	9.21	0.85
Y	-4.94	9.4	10.62	6.17
N	2.94	7.0	7.59	7.27
X_C	-0.52	7.0	7.02	6.00
Y_C	-1.99	9.4	9.61	9.43
N_C	1.42	7.0	7.14	5.67

Note: U_{SN} is the numerical uncertainty, U_D is the experimental uncertainty, and $\%\lvert E\rvert$ is the magnitude of the percentage error given in ITTC (2002a). These uncertainty values (U_V) were greater than the absolute value of the comparison error, $\lvert E\rvert$ as seen in Table A5 and thus the finest grid with 8.94M cells was utilized for the cases investigated in this study.

tions, iterative convergence, grid convergence, and time step convergence were selected and overall verification uncertainty was quantified for corrected and uncorrected results. This was then compared with the magnitude of the error to envisage the numerical accuracy of the CFD solutions.

APPENDIX B
EXPERIMENTAL SETUP

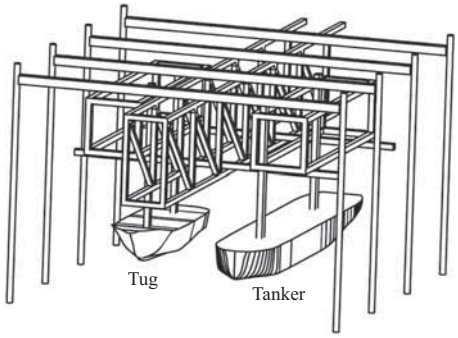

Fig. B1. Isometric View of the AMC model test basin's Drag-on arrangement.

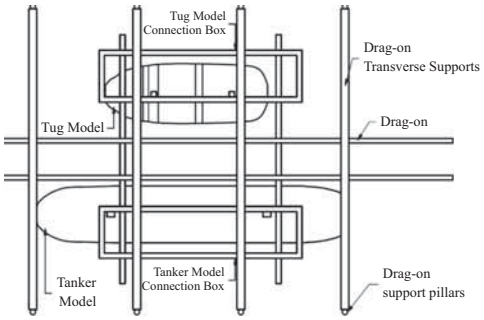

Fig. B2. Top View of the AMC model test basin's Drag-on arrangement.

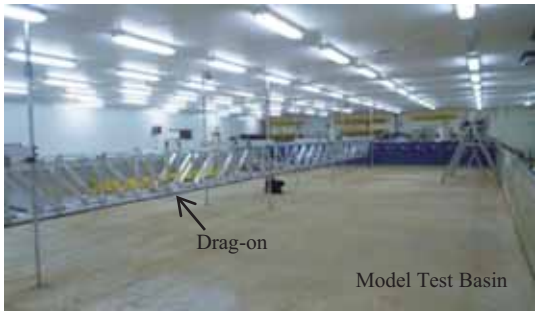

Fig. B3. Drag-on setup within empty Model Test Basin.

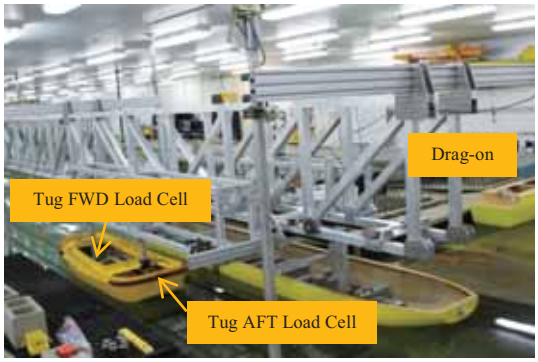

Fig. B4. Tug and tanker models with Drag-on and load cell arrangement.

Fig. B5. Parallel tug and tanker models during experiments.

Fig. B6. Drifted tug relative to tanker during experiments.

REFERENCES

CD-Adapco (2015). User Manual of StarCCM+ Version 10.02.

Dand, I. W. (1975). Some Aspects of Tug-Ship Interaction, in: Troup, K.D. (Ed.), The Fourth International Tug Convention, New Orleans, Louisiana, USA.

Falter, J. (2010). Validation of a Potential Flow Code for Computation of Ship-Ship Interaction Forces with Captive Model Test Results. Ghent University, Belgium, 86.

Fonfach, J. M. A. (2010). Numerical Study of the Hydrodynamic Interaction Between Ships in Viscous and Inviscid Flow. Instituto Superior Tecnico, Portugal, Portugal, 102.

Fonfach, J. M. A., S. Sutulo and C. G. Soares (2011). Numerical Study of Ship to Ship Interaction Forces on the Basis of Various Flow Models, in: Pettersen, B., Berg, T.E., Eloot, K., Vantorre, M. (Eds.), 2nd International Conference on Ship Manoeuvring in Shallow and Confined Water: Ship to Ship Interaction. RINA, Trondheim, Norway, 137-146.

Geerts, S., M. Vantorre, K. Eloot, R. Huijsmans and N. Fierens (2011). Interaction Forces in Tug Operation, in: Pettersen, B., Berg, T.E., Eloot, K., Vantorre, M. (Eds.), 2nd International Conference on Ship Manoeuvring in Shallow and Confined Water: Ship to Ship Interaction, Trondheim, Norway.

Gui, L., J. Longo, B. Metcalf, J. Shao and F. Stern (2000). Forces, Moment and Wave Pattern for Naval Combatant in Regular Head Waves, Twenty-Third Symposium on Naval Hydrodynamics. National Academy of Sciences, Val de Reuil, France.

Yoon, H., C. D. Simonsen, L. Benedetti, J. Longo, Y. Toda and F. Stern (2015a). Benchmark CFD validation data for surface combatant 5415 in PMM maneuvers-PartI: Force/moment/motion measurements. Ocean Engineering 109 (2015), 705-734.

Yoon, H., J. Longo, Y. Toda and F. Stern (2015b). Benchmark CFD validation data for surface combatant 5415 in PMM maneuvers-Par tII: Phase-averaged stereoscopic PIV flow field measurements. Ocean Engineering 109 (2015), 735-750.

Hensen, H. (2003). Tug Use in Port: A Practical Guide. Nautical Institute.

ITTC (2002a). CFD General Uncertainty Analysis in CFD Verification and Validation Methodology and Procedures. International Towing Tank Conference.

ITTC (2002b). Testing and Extrapolation Methods-Resistance Uncertainty Analysis. International Towing Tank Conference.

ITTC (2011). Ship Models, ITTC-ecommended Procedures and Guidelines. International Towing Tank Conference.

Jayarathne, B. N., D. Ranmuthugala, S. Chai and G. Fei (2014). Accuracy of potential flow methods to solve real-time ship-tug interaction effects within ship handling simulators. International Journal on Marine Navigation and Safety of Sea Transportation 8 (4), 497-504.

Leong, Z. Q., D. Ranmuthugala, I. Penesis and H. Nguyen (2014). RANS-Based CFD prediction of the hydrodynamic coefficients of DARPA SUBOFF geometry in straight-line and rotating arm manoeuvres. Transactions RINA: Part A1-International Journal Maritime Engineering.

Lindberg, O., H. B. Bingham, A. P. Engsig-Karup and P. A. Madsen (2012). Towards Real Time Simulation of Ship-Ship Interaction, The 27th International Workshop on Water Waves and Floating Bodies IWWWFB 2012, Copenhagen, Denmark.

MAIB (2011). Lessons from Marine Accidents, in: Hawes, J. (Ed.), Safety Digest. Marine Accident Investigation Branch, United Kingdom.

MCA (2001). Dangers of interaction. Maritime & Coastguard Agency, United Kingdom, 4.

Olivieri, A., F. Pistani, A. Avanzini and F. Stern. (2001). Towing Tank Experiments of Resistance, Sinkage and Trim, Boundary Layer, Wake and Free Surface Flow Around a Naval Combatant INSEAN 2340 Model, IIHR Technical Report No. 421. The University of Iowa, Iowa City, Iowa.

Pinkster, J. A. and K. Bhawsinka (2013). A Real-time Simulation Technique for Ship-Ship and Ship-Port Interactions, 28th International Workshop on Water Waves and Floating Bodies (IWWWFB 2013), L'Isle sur la Sorgue, France.

Salim, S. M. and S. C. Cheah (2009). Wall y^+ Strategy for Dealing with Wall-Bounded Turbulent Flows, International MultiConference of Engineers and Computer Scientists, Hong Kong.

Xun, S., X.-q. Chen and J.-h. Tan. (2010). Study of resistance performance of vessels with notches by experimental and computational fluid dynamics calculation methods. Journal of Shanghai Jiaotong University (Science) 15(3), 340-345.

Simonsen, C. D., C. K. Nielsen, J. F. Otzen and K. Agdrup (2011). CFD Based Prediction of Ship-Ship Interaction Forces on a Tug Beside a Tanker, in: Pettersen, B., Berg, T. E., Eloot, K., Vantorre, M. (Eds.), 2nd International Conference on Ship Manoeuvring in Shallow and Confined Water: Ship to Ship Interaction, Trondheim, Norway.

Sorensen, P. K., P. S. Jensen, B. Caspersen and J. H. Nielsen (2009). Latest Developments in the Use of Tug Simulation and Tug Simulation Technology, Tugnology '09, Amsterdam, Netherlands.

Sutulo, S. and C. G. Soares (2009). Simulation of close-proximity maneuvers using an online 3D potential flow method, international conference on marine simulation and ship maneuverability, Panama City, Panama, 558-567.

Sutulo, S., C. G. Soares and J. Otzen (2012). Validation of potential-flow estimation of interaction forces acting upon ship hulls in parallel motion. Journal of Ship Research 56(3), 129-145.

Tezdogan, T., Y. K. Demirel, P. Kellett, M. Khorasanchi, A. Incecik and O. Turan (2015). Full-scale unsteady RANS CFD simulations of ship behaviour and performance in head seas due to slow steaming. Ocean Engineering 97, 186-206.

Vantorre, M., E. Verzhbitskaya and E. Laforce (2002). Model test based formulations of ship-ship interaction forces. Ship Technology Research 49, 124-141.